

Mapping the Fields of Dipole and Quadrupole Magnets Procedure and Results

Reed Essick
Dr. Zikri Yusof
Argonne Wakefield Accelerator
Lee Teng Undergraduate Internship

Several new Radiabeam magnets will be installed in the Argonne Wakefield Accelerator (AWA) facility as part of the Emittance Exchange Experiment. The fields created by these magnets needed to be accurately mapped in three dimensions in order to correctly predict the trajectory of beam particles. To accomplish this, extensive measurements were made using dual Hall probes mounted on a positioning device. Procedures were developed and implemented to align both magnets to high precision using their fields. Field maps were created for one dipole and one quadrupole. Multiple transverse and longitudinal measurements were conducted on each magnet to fully characterize their fields. The mapped fields were then used in a numerical simulation to predict the path taken by a single relativistic electron with a well defined initial position and momentum. Field mapping facilitated computation of pertinent properties of the magnets, such as effective lengths, and allowed vendor data to be verified.

Mapping the Fields of Dipole and Quadrupole Magnets: Procedures and Results

Several new magnets are to be installed in the Argonne Wakefield Accelerator (AWA) facility as part of the Emittance Exchange Experiment. The fields of two of these magnets were extensively mapped to confirm vendor simulations and to calculate their effective lengths. Both magnets were manufactured by Radiabeam Technologies. A dipole (EMD-01-201-787) and a quadrupole (EMQR-03) were studied. While both magnets were designated for use in the Emittance Exchange Experiment, the quadrupoles may be employed as part of the new AWA beamline. Measurements were made with two hall probes manufactured by Group 3 Technologies. The probe tips (MPT-231) had an active area of 1.0 mm x 0.5 mm and were accurate to five hundredths of a Gauss. The probes were coupled with digital teslameters (DTM-141), one per probe, from which readings were taken. Both probes were mounted so that they measured the same field component and were located on at the end of the meter long arm attached to the positioning device. The device was a Compumotor 4000 Motion Controller, capable of motion in three mutually orthogonal directions. The probe arm could also rotate 360° about its axis. Field variation was measured as a function of both transverse and longitudinal motion, as well as a function of current per coil supplied to the magnet.

Several different power supplies were used to make these measurements. The supply used was chosen based on its stability and range. All measurements were made using current controlled supplies held at a constant current. During saturation measurements, the current was changed quickly and then held constant while the measurements were made. It was often necessary to wait for extended periods before recording data to ensure that transient effects had damped out.

A numerical simulation was run through MatLAB using measured data to predict the trajectory of beam particles. A space-stepping procedure was implemented in order to achieve this. Trajectories were mapped for particles passing through the measured dipole field, and from this the effective length of the dipole (for a bend angle of $\theta = 20^\circ$) was calculated. Other pertinent properties of the magnets were calculated using MatLAB as well, such as the effective length of the quadrupole.

Field Mapping

The positioning device was leveled with the magnets using adjustable feet, and was capable of motion in three mutually orthogonal directions. It could be directed either with a local controller or remotely by computer. Data was taken both by hand and using an automated program. The apparatus was constructed for use in the Advanced Photon Source (APS) facility, and was on loan to AWA.

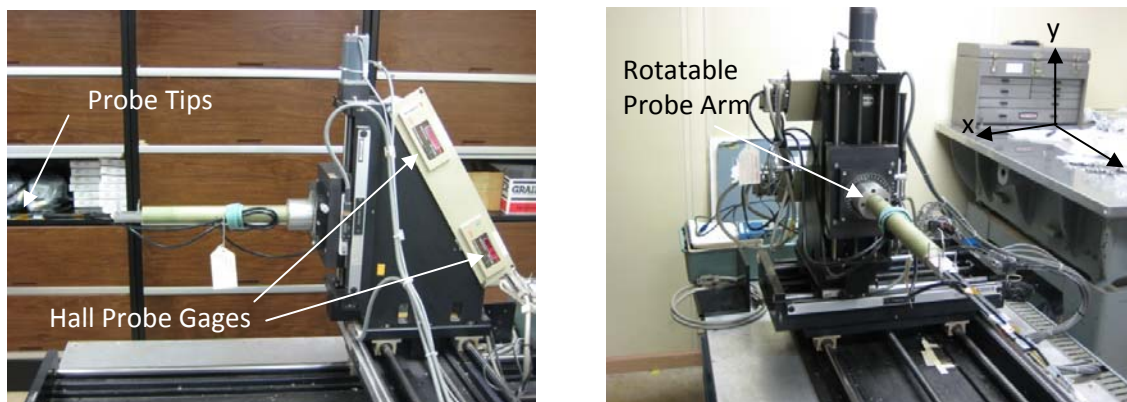


Figure 1: Hall Probe Positioning Device

To compensate for any ambient field, several measurements were normalized using a hand held gauss-meter. The dual probes were zeroed far away from the magnet, and then the ambient field at that point was measured with the handheld gauss-meter. This was necessary because the zero-gauss chamber was not large enough to hold the dual probes. There was some ambiguity in that rotation of the handheld meter by 180° resulted in a polarity change of the field, and it was not immediately clear which polarity was correct. It was decided that the polarity should match that of the dual probes when they are measuring an induced field.

The two hall probes were mounted in such a way that they should measure the same component of the field. However, the two probes were not exactly parallel. This gave rise to complications in determining exactly which component of the field was measured.

Dipole

A Radiabeam dipole was thoroughly mapped using the hall probe device. Longitudinal and transverse scans were conducted with the two coils of the dipole wired in series. Vendor specifications state that the dipole should be run at 11.8 A/ 23.6 V. Due to power supply limitations, the maximum current achievable at the time of measurement was 10.0 Amp. All scans were run at 10.0 Amp, provided by a current regulated power supply, with the exception of the saturation measurement.

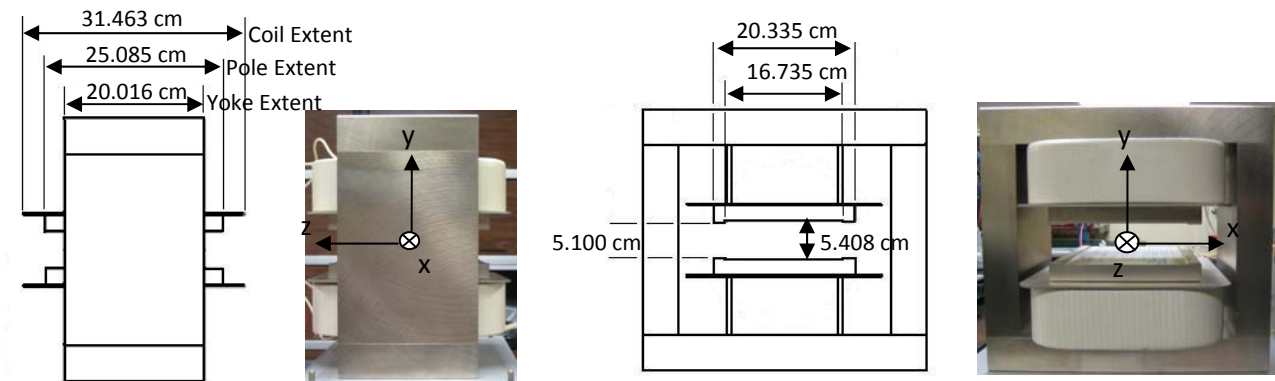


Figure 2: Physical Parameters of Dipole

Leveling and Centering Procedure

The magnet was set on an adjustable table, and then leveled to the hall probe device (i.e.: to gravity). The center of the magnet was found by using the positioning device to measure the distance between the walls of the magnet. Since the field was not supposed to vary within the magnet, these simple measurements were deemed sufficiently accurate. All motion was made relative to the center position once it was defined.

A more accurate way to locate the center of the magnet would be to find positions that read the same magnitude for the field, one on either side of the center. The center point of the line connecting these points should be the center of the magnet. For this procedure, it would be important to choose points that are far enough from the center that they are not on the plateau portion of the field. By choosing appropriate points along each of the three spatial axes, the center of the magnet could be found to high accuracy.

Once the magnet itself was level, the longitudinal axis alignment was checked by placing the probe tip near one wall and jogging in the longitudinal direction and verifying that the distance between the probe and the wall remained constant. The longitudinal alignment is important for the

dipole, but not as important as for the quadrupole. Therefore, this alignment by eye sufficed for the measurements made.

As the Field was expected to only have a vertical component, the fact that the probes did not measure exactly the same component was taken into account by rotating the probe arm until their magnitudes were equal. By symmetry, their average should then lie directly on the vertical component. The actual components measured will be nearly parallel to the vertical and so the small rotation will be negligible.

Saturation Measurements

A saturation measurement was also made for the dipole magnet. Current was increased monotonically to 10 Amps, decreased to -10 Amps and then returned to 0 Amps. The extent of this measurement was limited by the power supply available at the time.

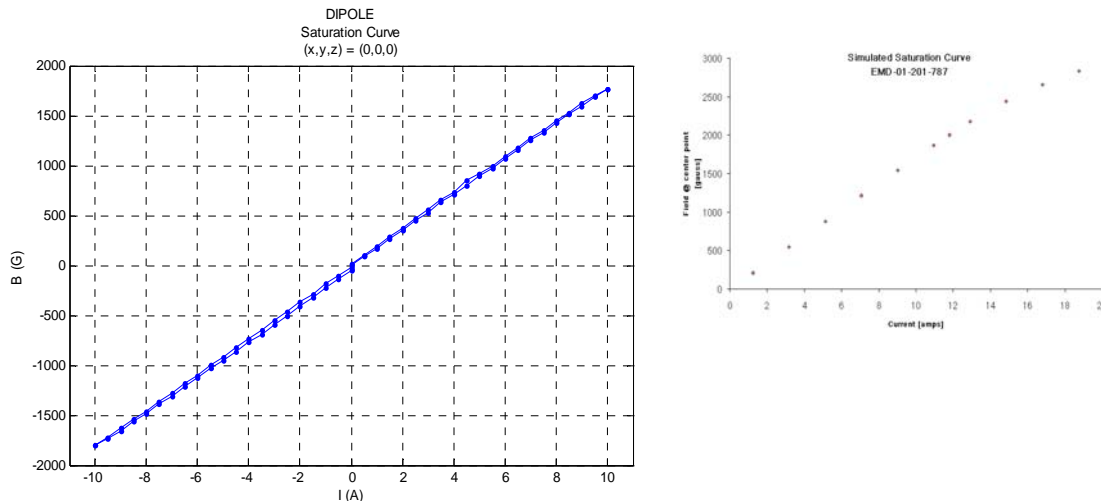


Figure 9: Saturation Curve for Dipole (Measured and Simulated)

While there is some evidence of hysteresis, the differences between the two curves are small. Likewise, there is no saturation of the iron yoke up to 10 Amps.

Longitudinal Measurements

Longitudinal scans were conducted on-axis, and compared with the simulations run by the vendor. The measured fields matched those predicted by the vendor to high accuracy.

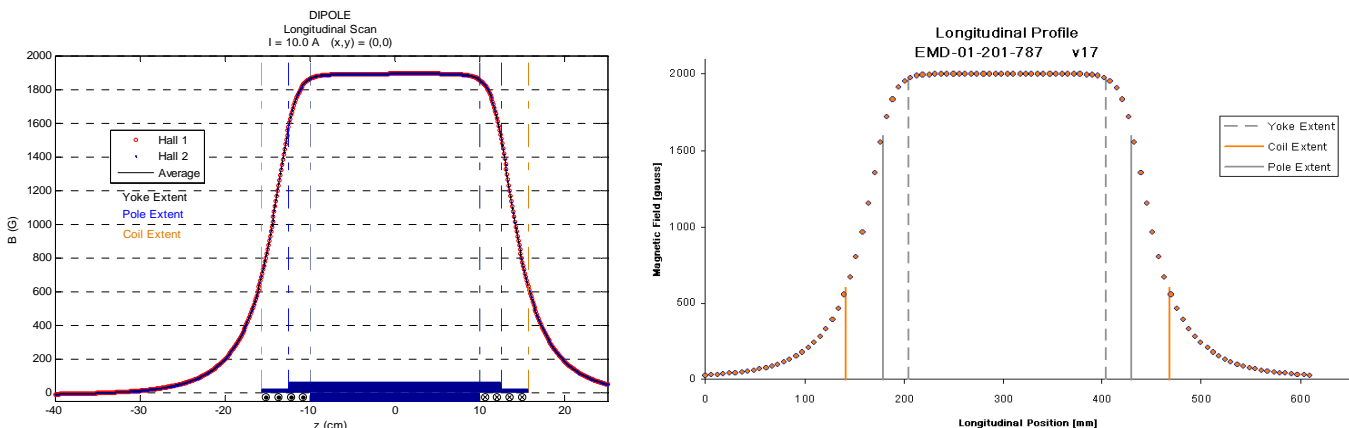


Figure 3: Longitudinal Variation of Field (Measured and Simulated)

Both probe values are plotted as well as their average. Noise is negligible as all three plots fall on top of one another. The characteristic plateau profile is observed, with the field relatively tightly confined to within the magnet's coils.

Transverse Measurements

In addition, transverse scans were made of the magnetic field. A horizontal scan was made from the center of the magnet, and several vertical scans were conducted at different horizontal positions, all centered longitudinally.

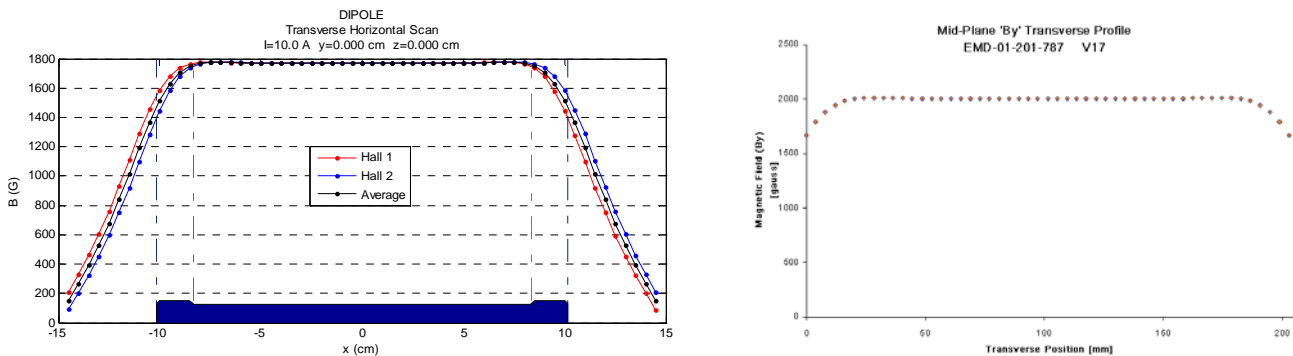


Figure 4: Horizontal Transverse Scan (Measured and Simulated)

The field is tightly constrained to within the magnet's pole and shows the plateau profile as well. The steep drop off is caused by the raised edges of the pole. Also note that near the sides of the measurement, the physical separation of the two hall probes is enough to cause their readings to differ significantly. By averaging the values, this is taken into account. The average value is symmetric.

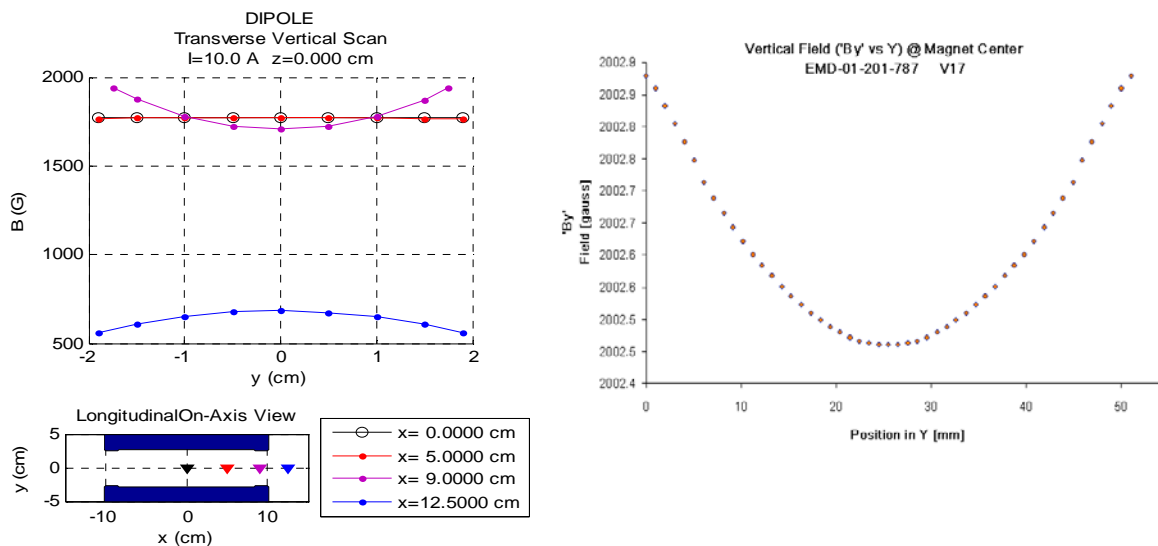


Figure 5: Vertical Transverse Scan (Measured and Simulated)

These scans show that the field strength does not vary significantly within the yoke of the magnet. The values taken at $x=0.00$ cm and $x=5.00$ cm fall nearly on top of one another. Likewise, the parabolic shape predicted by the vendor is seen clearly in the measurement at $x=9.00$ cm. This trend is also visible at $x=0.00$ and $x=5.00$, but the variation is insignificant compared to the peak

field. The trend is visible in the vendor simulation because the scale is much finer. Also, the curvature of the field over vertical motion is reversed once outside of the pole, as shown by the measurement at $x=12.50$ cm. This is due to the fact that when the probes are within the pole's extent, the field is concentrated near the pole surface. However, outside the pole the probes measure a component of the field parallel to conductor's surface. Therefore, near the top and bottom of the vertical range the probes are parallel to a conductor and the field decreases.

Planar Scans at Fixed Elevations

Several maps of one octant of the dipole were conducted. Three horizontal planes were mapped. This data was built into a three dimensional lattice assuming symmetry throughout the dipole. The lattice was then used by the simulation to calculate the trajectory of a beam particle. The sample rate of these measurements was low compared to other measurements made. For example, only three elevations were mapped. This was deemed sufficient since the field is highly symmetric and varies extremely slowly over vertical displacement.

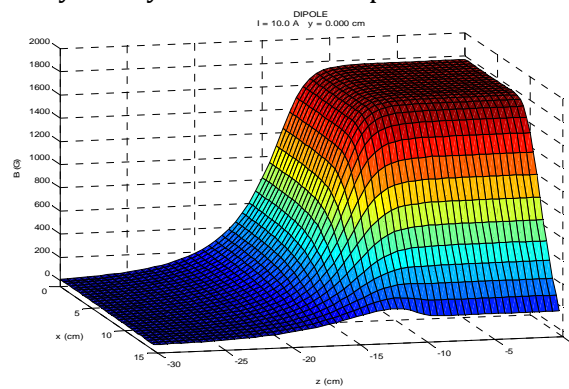


Figure 6: Octant Scan at $y=0.000$ cm

This figure plots the magnetic field as a function of x and z positions. It is clear that the dipole displays the characteristic plateau. An interesting feature is the small increase in field strength near $(x, z) = (14, -15)$. This is caused by the probe tip leaving the interior of the magnet. Near the yoke of the magnet, the field is driven to zero. However, when the probe leaves the inside of the magnet, the field is no longer suppressed in this way.

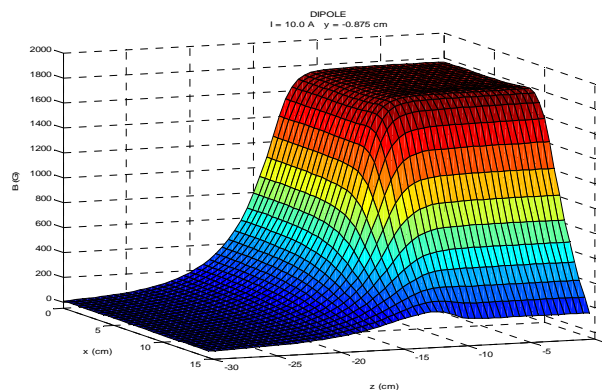


Figure 7: Octant Scan at $y=-0.875$ cm

This scan is nearly identical to the previous scan, showing that the field maintains the same properties over a range of elevation. There is a small fringe field near $x=9.000$ cm, which corresponds to raised edge of the magnet pole. The probe is closer to the pole along this line, which drives the field higher. However, the change is not significant and is outside the region that will contain beam.

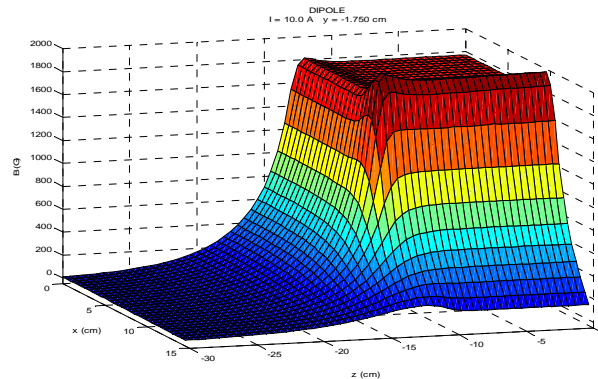


Figure 8: Octant Scan at $y=-1.750$ cm

While this scan shows the same overall features as the others, the edge effects are much more pronounced as the probe is closer to the pole. Since the pole ends abruptly, there is field concentration around the sudden change. This can be seen by the ridges at the edges of the plateau. The ridge running longitudinally is higher because it is also caused by the raised edge of the pole.

Dipole Effective Length

The effective length (L_e) of the dipole is calculated by an integral along the path taken by the beam's center of mass as it passes through the dipole field.

$$L_e = \frac{1}{B_{\max}} \int_{-w}^{w} B ds$$

The fact that the beam bends complicates the integral, as the trajectory no longer lies along the z axis. To calculate the effective length, it was necessary to first solve numerically for the trajectory taken by one particle through the dipole field. This was accomplished using a space-stepping procedure, with magnetic field values interpolated from the data taken above. The position at each step was stored along with the magnitude of the magnetic field. Using these computed values, an approximation to the integral ($\int_{-w}^{w} B ds$) was performed and then normalized using the peak field value (B_{\max}). This yielded the reported value of the effective length, which is just beyond the physical extent of the magnet.

$$L_e = 31.54 \text{ cm}$$

The effective length varied with the bend angle, and this value is for a 20° bend. The step size used was 2.5 mm, which is half the distance between field measurements. Using a smaller step size than this did not increase accuracy with the precision reported.

To achieve this bend angle, either the momentum of the particle or the strength of the field could be varied. Each approach was implemented, and for the same bend angle they produced the same effective length. This should have been expected as the trajectory was the same for each case and the strength of the field was normalized by the peak field.

Quadrupole

A new Radiabeam quadrupole was also studied. The four coils were wired in series, and run using a current controlled power supply. All measurements were made at 9.0 Amp, with the exception of the saturation measurement. Vendor specifications indicate that the quadrupole should be run at of 9.0 A/16.9 V. The inner bore of the quadrupole was two inches in diameter, which is the size of the beampipe used in the AWA.

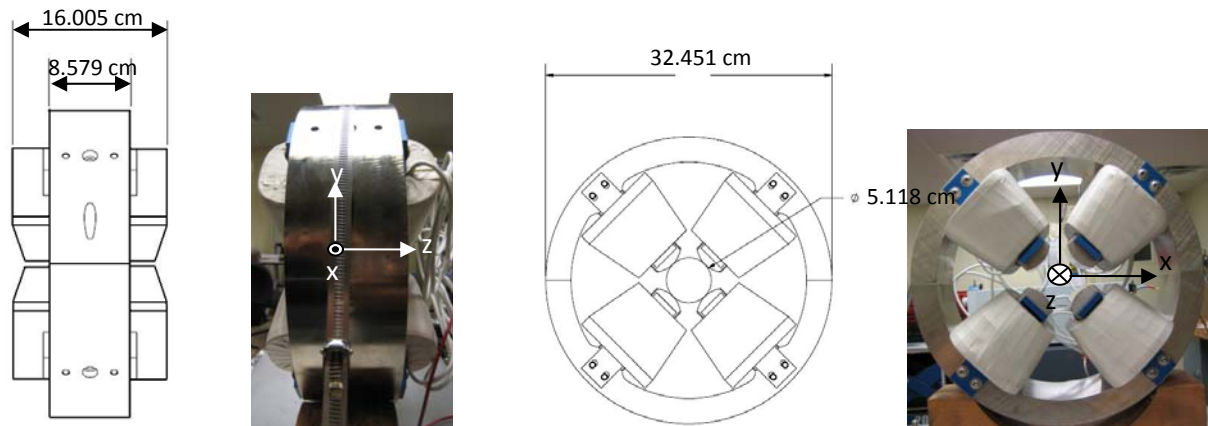


Figure 10: Physical Parameters of Quadrupole

Centering Procedure and Longitudinal Axis Alignment

First, the magnet yoke was leveled to the machine (i.e.: to gravity). Then, the rotation of the magnet about the longitudinal axis was leveled with some reproducible marking. These quadrupoles could be split into hemispheres, and the joint between the halves was used. At this point the magnet should have been leveled with the machine in all planes except for yaw and an attempt was made to match the yaw as closely as possible by eye. However, accuracy was improved by making use of the quadrupole field. Error was detected by the two probes in the following way. If the longitudinal axis of the device was indeed aligned with that of the magnet, then when the probe was on center the two readings should be of the same magnitude, but of opposite sign. The probes were positioned so that they were in the center of the magnet. They were then moved to some positive longitudinal position, and the magnet was twisted in yaw to correct for any error. It was found that two C-clamps, one on either side of the magnet, could be used to incrementally move only one side of the magnet, thereby twisting it in yaw.

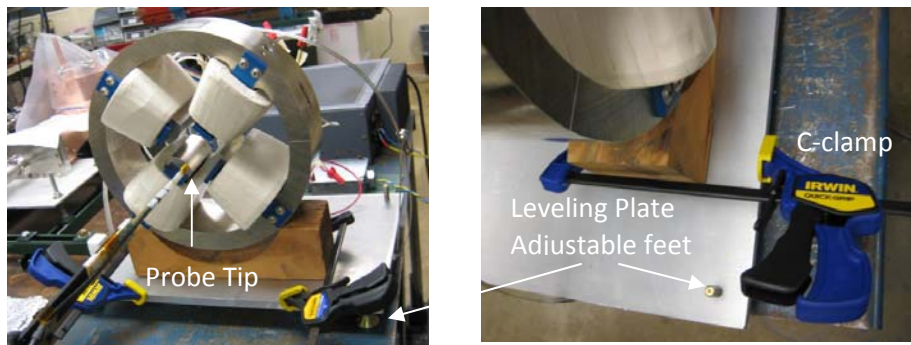


Figure 11: Quadrupole Positioning Hardware



Figure 12: Quadrupole Alignment Directions

Once the magnet was been twisted, the probes were moved to the other side of the magnet (if they were at a positive longitude, they were moved to a negative longitude). By recognizing which value is larger absolutely, the magnets twist could be inferred. (The probe with the larger value was closer to a pole.)The twist was corrected manually and then the probe was re-centered. To re-center the probe, the device was jogged transversely until the measured magnitudes were equal. After each adjustment was made to the magnet, it was crucial that the probe be re-centered. The probes were then moved to the other side of the magnet and the process repeated. It was prudent to move the magnet minimally to avoid over-compensation.

After some number of repetitions, the yaw was aligned to within the desired precision. Since high gradient is desirable in a quadrupole, proper alignment can be achieved to high accuracy. However, the high gradient also implies that small errors affect measured data significantly and accuracy will most likely be limited by the ability to position the magnet. The positioning device was accurate to within 10 microns, which corresponds to an error of 0.9399 Gauss using the measured gradient. For this measurement, the alignment was adjusted until the magnitudes differed by around 0.3 Gauss after translation through nearly 20 centimeters. At this point, the measurement of $B_y(x=1, y=0)$ was conducted over a large range of z values. The probe was re-centered for the measurement of $B_x(x=0, y=1)$, but the magnet was assumed to be aligned properly as it was previously leveled in this plane.

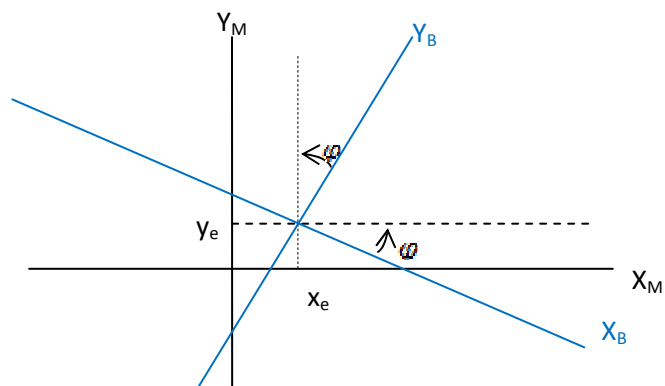
Resolution of the Skew Angle and Centering Errors

Even though the steel yoke of the magnet (M frame) is level with the measurement instrument, there may be errors causing the field to be skewed through some angle. Therefore, motion along one axis in the M frame does not correspond to motion along a single axis in the field's true frame (B frame). Therefore, the known field equations that apply in the true frame must be converted into the mechanical frame in which measurements are made. This assumes that the longitudinal axes in both frames are parallel.

From the figure shown

$$\begin{bmatrix} x_B \\ y_B \end{bmatrix} = \lambda_R \begin{bmatrix} (x_M - x_e) \\ (y_M - y_e) \end{bmatrix}$$

where $\lambda_R = \begin{bmatrix} \cos \varphi & -\sin \varphi \\ \sin \varphi & \cos \varphi \end{bmatrix}$



Likewise, the field components transform as

$$\begin{bmatrix} B_{x_m} \\ B_{y_m} \end{bmatrix} = [\lambda_B^{-1}] \begin{bmatrix} B_{x_B} \\ B_{y_B} \end{bmatrix}$$

Now, for a quadrupole magnet, the field in the B frame is known to be

$$\begin{bmatrix} B_{x_B} \\ B_{y_B} \end{bmatrix} = \begin{bmatrix} ky_B \\ kx_B \end{bmatrix} \text{ where } k = \text{Magnetic Field Gradient}$$

Knowing this, it can be shown that

$$\begin{bmatrix} B_{x_m} \\ B_{y_m} \end{bmatrix} = [\lambda_B^{-1}] \begin{bmatrix} ky_B \\ kx_B \end{bmatrix} = k \begin{bmatrix} \cos \varphi & \sin \varphi \\ -\sin \varphi & \cos \varphi \end{bmatrix} \begin{bmatrix} (x_M - x_e) \sin \varphi + (y_M - y_e) \cos \varphi \\ (x_M - x_e) \cos \varphi - (y_M - y_e) \sin \varphi \end{bmatrix}$$

$$\begin{bmatrix} B_{x_m} \\ B_{y_m} \end{bmatrix} = k \begin{bmatrix} (x_M - x_e)(2 \sin \varphi \cos \varphi) + (y_M - y_e)(\cos^2 \varphi - \sin^2 \varphi) \\ (x_M - x_e)(\cos^2 \varphi - \sin^2 \varphi) - (y_M - y_e)(2 \sin \varphi \cos \varphi) \end{bmatrix}$$

Simplification yields

$$B_{x_m} = k[\sin 2\varphi (x_M - x_e) + \cos 2\varphi (y_M - y_e)] \quad \text{and} \quad B_{y_m} = k[\cos 2\varphi (x_M - x_e) - \sin 2\varphi (y_M - y_e)]$$

Now, taking the partial derivative with respect to x_M of both components, produces

$$\frac{\partial}{\partial x_M} B_{x_m} = k \sin 2\varphi \quad \text{and} \quad \frac{\partial}{\partial x_M} B_{y_m} = k \cos 2\varphi$$

A unique solution can be determined from these equations. Solving for k and φ yields

$$(k)^2 = \left(\frac{\partial}{\partial x_M} B_{x_m} \right)^2 + \left(\frac{\partial}{\partial x_M} B_{y_m} \right)^2 \quad \text{and} \quad \varphi = \frac{1}{2} \tan^{-1} \left(\frac{\frac{\partial}{\partial x_M} B_{x_m}}{\frac{\partial}{\partial x_M} B_{y_m}} \right)$$

Note that this is independent of the locations of the coordinate origins. To solve for x_e and y_e , measurements of both B_{x_m} and B_{y_m} must be made at $\begin{bmatrix} x_M \\ y_M \end{bmatrix} = \begin{bmatrix} 0 \\ 0 \end{bmatrix}$. This could be done as part of the scan to find the values of k and φ . Solving for k and φ and substituting into the equations for B_{x_m} and B_{y_m} will yield solutions for x_e and y_e as shown.

$$x_e = -\frac{1}{k} [B_{y_m} \cos 2\varphi + B_{x_m} \sin 2\varphi] \quad \text{and} \quad y_e = \frac{1}{k} [B_{y_m} \sin 2\varphi - B_{x_m} \cos 2\varphi]$$

Therefore, the orientation and position of the true frame with respect to the mechanical frame can be uniquely determined if scans are made of B_{x_m} and B_{y_m} at $y_M = 0$ and through an appropriate range of x_M that includes $x_M = 0$. Finding these last error terms also allows for a computation of the dipole error induced by the quadrupole at its measured location.

Saturation Measurements

An attempt to measure the radial component of the field at the pole tip was made during this saturation measurement. However, the dual probes did not lie exactly on the axis of rotation of the arm. Therefore, when trying to make one hall probe parallel to the pole, simple rotation of the probe arm would not suffice. As the arm rotated, the probes moved closer to/further from the magnet tip, and did not simply rotate about their own axes. Furthermore, the two probes were not exactly parallel. The probe was positioned by eye to be parallel to the magnet tip at its center, and then rotation was used to equate the values read out by the hall probes. While the probes measured different components of the field, their average should lie directly on the radial line. This must be true by the symmetry of the field, that is, if the center of the arm is directly on the radial line of the magnet. Likewise, it was difficult to position the probe exactly at the pole tip, and measurements were made about one centimeter from the pole.

Motion in the proximity of the quadrupole while the measurement was made increased uncertainty as the values fluctuated depending on their surroundings. It was necessary to wait for approximately one minute after adjusting the current to allow the values to settle down. At 15 A and above, the power supply was near its maximum output and values began to fluctuate more.

For this measurement, current was decreased monotonically from 0.0 A to -16.5 A (limited by power supply), then increased monotonically to 16.5 A and finally decreased back to 0.0 A.

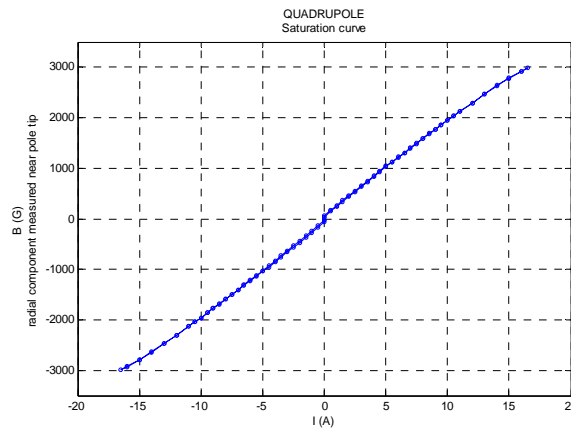


Figure 13: Field Saturation Curve for Quadrupole

Note that there is some hysteresis present, as well as residual magnetization when the current vanishes. The yoke does not begin to saturate until above 10.0 A, which is beyond the planned operating environment for this magnet.

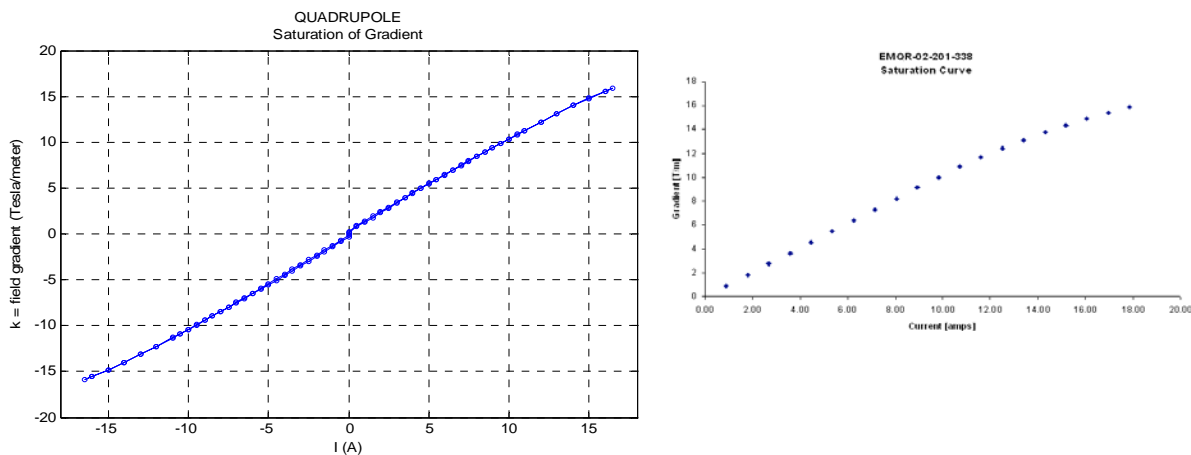


Figure 14: Gradient Saturation Curve (Measured and Simulated)

This plot was created using the saturation curve of the radial field normalized to the magnitude of the field at 9.0 Amp of current. Multiplying this normalized curve by the measured gradient at 9.0 Amp yielded the above curve. This follows because the geometry of the field is set by the shape of the poles, while the magnitude of the field depends on the current. We therefore expect the field to look like:

$$\begin{bmatrix} B_x \\ B_y \end{bmatrix} = f(I)k \begin{bmatrix} y \\ x \end{bmatrix}$$

where $f(I)$ is some function of the current and k is the field gradient. To find the saturation of the gradient, we take the partials of B_x and B_y

$$\frac{\partial B_y}{\partial x} = \frac{\partial B_x}{\partial y} = f(I)k$$

Therefore, the functional form of $f(I)$ that is measured in $B(I)$ would be observed in $\frac{\partial B_y}{\partial x}(I) = \frac{\partial B_x}{\partial y}(I)$. By normalizing the plot of $B(I)$ and then multiplying by the known gradient at 9.0 A, the variation of the gradient with current can be accurately plotted. Again, this confirms the vendor simulation nicely

Longitudinal Measurements

There was some uncertainty in the value of the transverse coordinates in these measurements. Since the probe did not sit exactly on the axis of the arm, when it was rotated to measure the other component, the actual location of the probe in both transverse directions was not what it was before rotation. However, this was not a reason for concern. As long as the fixed coordinates remained fixed, they simply acted as a coefficient that modulated the peak values measured.

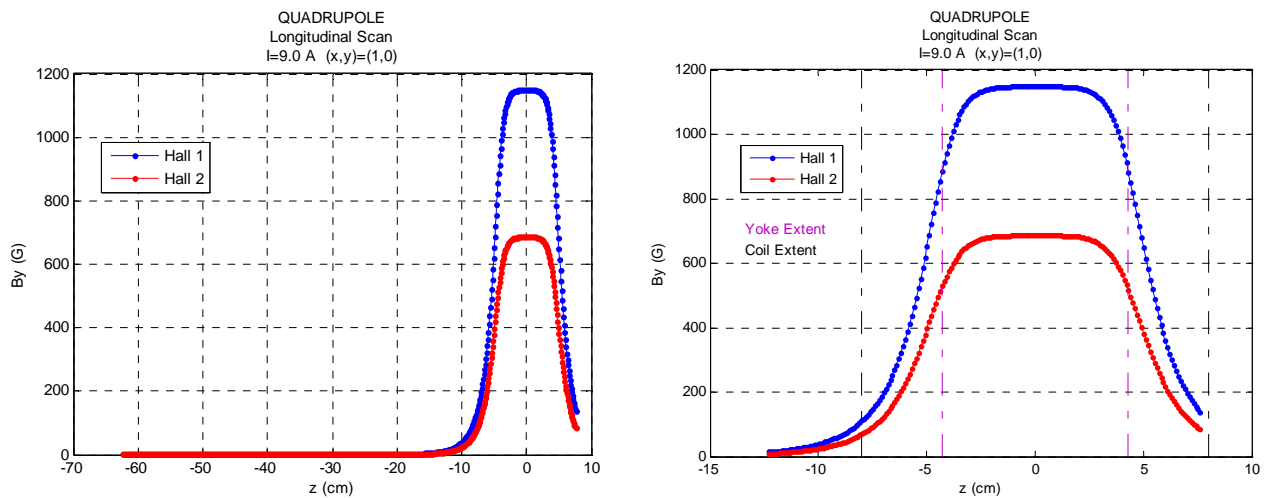


Figure 15: Longitudinal Variation of B_y at $(x, y) = (1, 0)$

This data shows that the quad is leveled correctly, as the plateau is indeed a plateau. Note that the two probes reach different peak values. This is because all Hall 2 was closer to the center of the magnet than Hall 1 during the measurement.

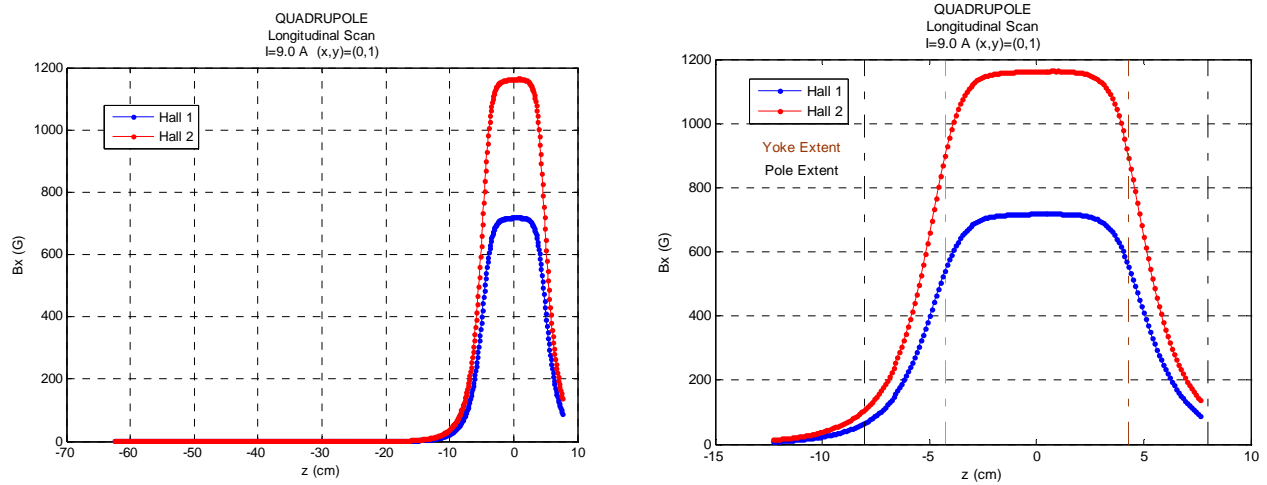


Figure 16: Longitudinal Variation of B_x at $(x, y) = (0, 1)$

This data seems to show that the quad was not exactly leveled. However, the error appears to be small, and perhaps negligible considering the difficulty inherent in aligning the quadrupole. Note that B_x and B_y show very similar behavior, as expected. They also match the vendor simulation, which is shown below.

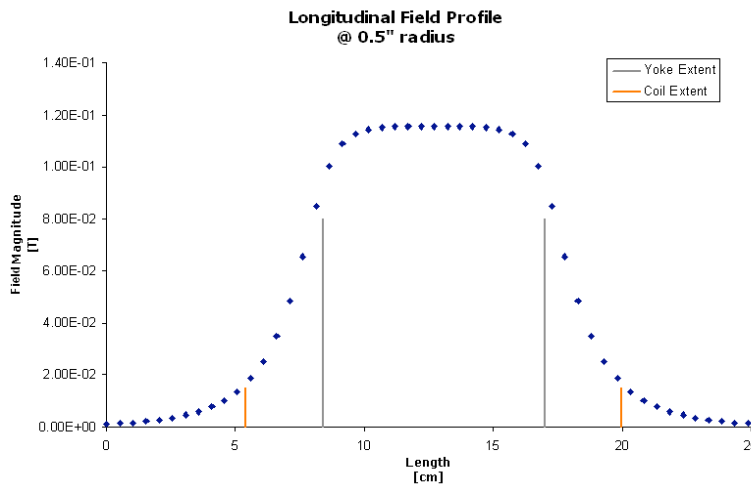


Figure 17: Vendor Simulation of Longitudinal Variation

Quadrupole Effective Length

To calculate the quadrupole's effective length (L_e), an integration was performed as shown

$$L_e = \frac{1}{B_{THEORY}} \int_{-\infty}^{\infty} B ds = \frac{1}{B_{THEORY}} \int_{-\infty}^{\infty} B dz$$

where ds is the path element of the trajectory of the beam's center of mass. Since the beam is focused and not bent, this corresponds to the longitudinal axis. Performing this integration for all

four sets of data taken (two hall probes each measuring over B_x and B_y) yielded the following effective lengths

$$\begin{aligned} (L_{e1})_x &= 10.9837 \text{ cm} \\ (L_{e2})_x &= 11.0004 \text{ cm} \\ (L_{e1})_y &= 10.9480 \text{ cm} \\ (L_{e2})_y &= 10.9585 \text{ cm} \end{aligned}$$

These values agree to within 53 μm , which is on the order of the error in positioning the hall probes. The average effect length is then

$$\begin{aligned} (L_e)_{\text{average}} &= 10.9726 \text{ cm} \\ &= 4.31994 \text{ in.} \end{aligned}$$

Measurement of Gradient

Ideally, the gradient could be computed immediately from the dual hall probes, if the separation between the active regions was known and they measured exactly the same component of the field. However, the two probes used were not exactly parallel and would therefore measure different components. This prohibits the computation of the gradient as laid out above. Instead, the gradient was measured by stepping the probe a known distance transversely. Then, a gradient was calculated from each of the hall probes independently. If the angle between the probes was small, then the two gradients calculated from each probe should be nearly identical.

A measurement was made of each component as it varied over the appropriate transverse direction. Gradients were then computed from best fit lines and averaged to produce the reported value.

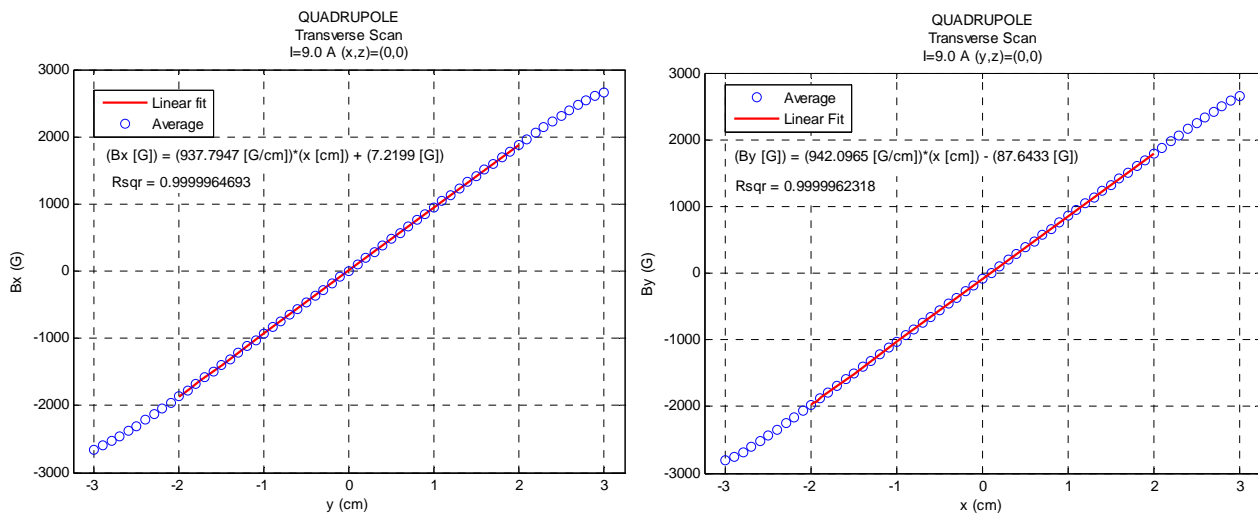


Figure 21: Gradient Measures from Transverse Scans: B_x through y and B_y through x

$$\begin{aligned} k_{\text{average}} &= 939.9456 \text{ Gauss/centimeter} \\ &= 9.399456 \text{ Tesla/meter at } I = 9.0 \text{ Amp} \end{aligned}$$

The reported value is extremely close to the value computed along with the skew angle, with only a 1.014% difference between the two. It is expected that this measurement is more accurate because the signal to noise ratio is much better. The difference may also be accounted for by differences in the supplied currents, although this contribution should be small.

Resolution of Skew Angle in Quadrupole

If the field was rotated relative to the mechanical frame to which the positioning device was leveled, then motion along one axis in the mechanical frame would correspond to motion along some combination of both axes in the field's frame. This variation should then be detectable. In order to measure the error between the magnet yoke's alignment and the field alignment, the skew angle resolution procedure was carried out when the yoke was leveled to the positioning device.

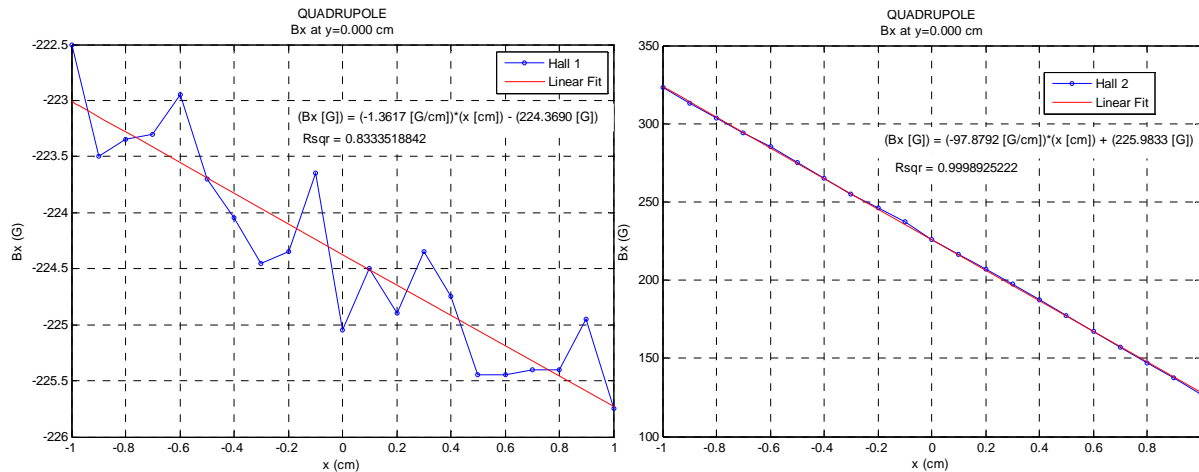


Figure 18: Transverse Variation of B_x over x

It is evident that the two hall probes were not exactly parallel. Hall 1 was leveled with the positioning device. However, Hall 2 was not. This accounts for the difference in the gradients, as Hall 2 measured part of a component that changed with respect to x , whereas the desired component should not (for a small skew angle). Because of this, the following analysis uses only the data taken from Hall 1.

There is significant noise in the Hall 1 data. This could be attributed to mechanical vibrations caused by the power supply or the positioning device. The probe tip is at the end of a meter long arm, and small vibrations at the base could be amplified at the end of that arm. It could also be the wriggle in the DC current supplied to the quadrupole.

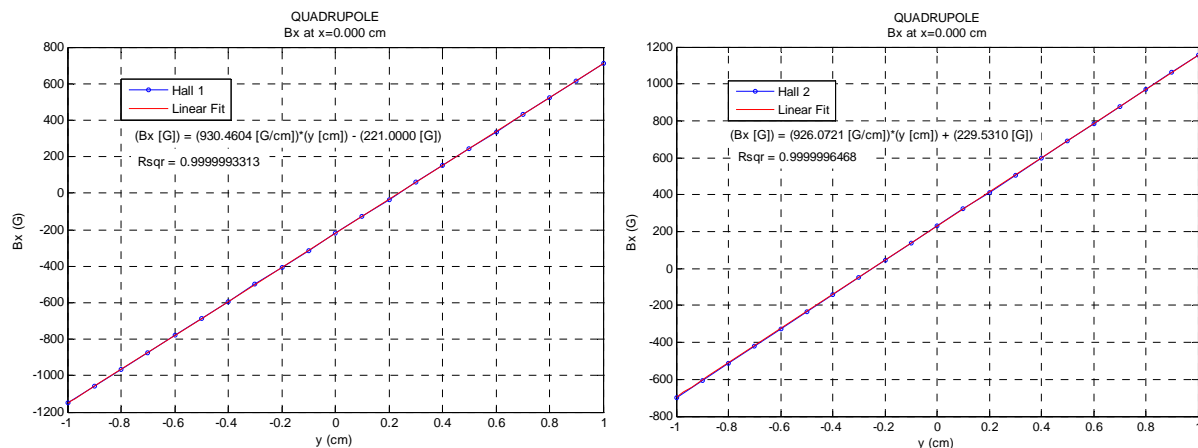


Figure 19: Transverse Variation of B_x over y

Since the field is expected to vary in this direction, the noise is greatly reduced. Likewise, the fact that the two probes did not measure exactly the same component is hidden in the large range seen by both probes. This is seen in that both figures have extremely well fit lines.

Now, using the data from Hall 1, we have that

$$\varphi = \frac{1}{2} \tan^{-1} \left(\frac{-1.3617}{930.46} \right) = -7.3173(10^{-4}) \text{ radians} = -0.041925^\circ$$

$$(k)^2 = (-1.3617)^2 + (930.46)^2 \rightarrow k = 930.461 \text{ Gauss/centimeter}$$

$$= 9.30461 \text{ Tesla/meter at } I = 9.0 \text{ Amps}$$

To confirm that the procedure outlined above is indeed accurate, the quadrupole was rotated about its longitudinal axis through an arbitrary angle. This angle was measured to be 15° using a Miracle Point Mercury Balance temporarily attached to the side of the yoke. Measurements were then made of B_y over both transverse directions, and the gradients along those directions were computed from best fit lines. Again, only data from Hall 1 was used.

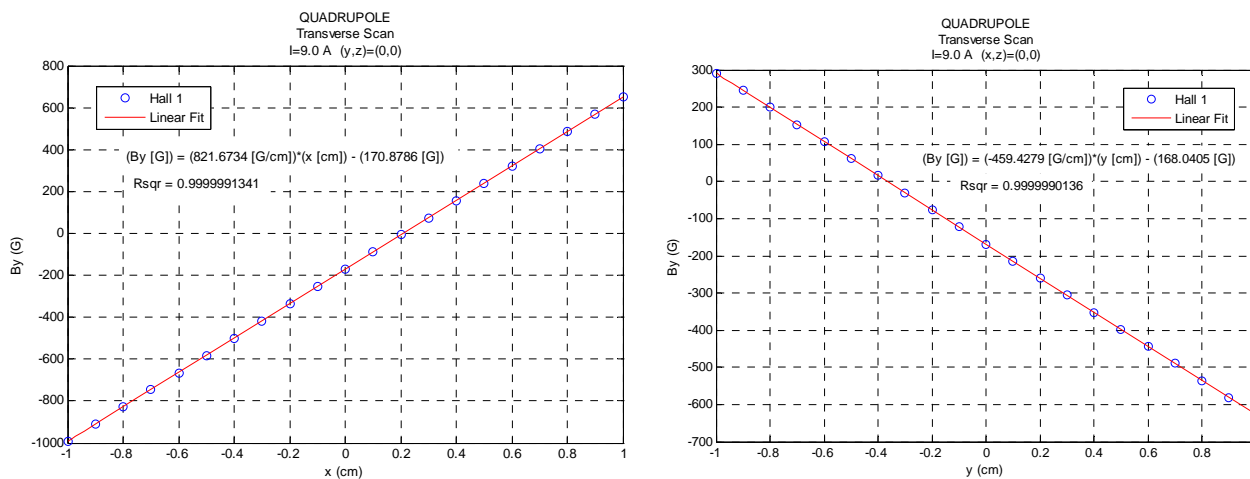


Figure 20: Transverse Scans of B_y in Rotated Quadrupole

Using the relations derived previously, it can be shown that

$$\varphi = \frac{1}{2} \tan^{-1} \left(\frac{\frac{\partial}{\partial x} B_{ym}}{\frac{\partial}{\partial y} B_{xm}} \right)$$

$$= \frac{1}{2} \tan^{-1} \left(-\frac{459.4279}{821.6734} \right) = 14.60556^\circ$$

There is only 2.7% difference between the known angle and this result. This validates the accuracy of this procedure in determining the skew angle of the quadrupole. Likewise, the gradient was computed from this data and found to be

$$k = 941.3931 \text{ Gauss/centimeter}$$

There is only a 0.15% difference between this value and the value reported under Measurement of Gradient. This suggests that the computed skew angle is more accurate than the one read on the mercury balance.

Transverse Planar Scan at Center of Quadrupole

To gain a better visualization of the field within the quadrupole, measurements were made of both B_x and B_y on the transverse plane at $z = 0.000$ cm. These measurements were then plotted using MatLAB to yield the following figures.

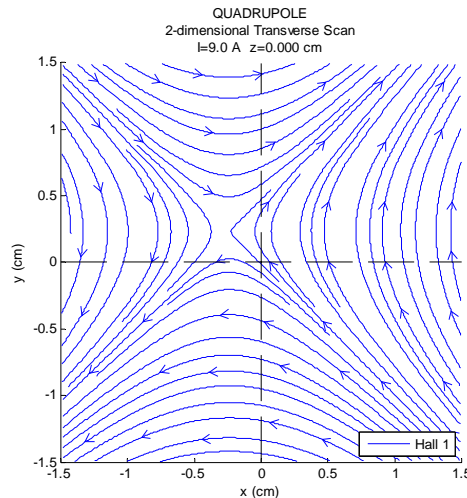


Figure 22: 2D Transverse Scan at $z=0$ (Hall 1)

As Hall 1 was leveled to the arm of the positioning device, it could be leveled with gravity and therefore leveled with the magnet. This is seen in the figure as the field looks exactly as expected, except for an origin mismatch. That mismatch was caused by the finite width of the probe. Since the probe tip really contained two probes, each measuring at some distance from the center of the arm, when the arm is centered in the magnet each probe is not. Knowing this, we can see that Hall 1 was about 2.5 mm off center of the arm, as it was displaced by that amount in the negative y direction and in the positive x direction. The displacement is seen in both directions because the arm was rotated to measure each component.

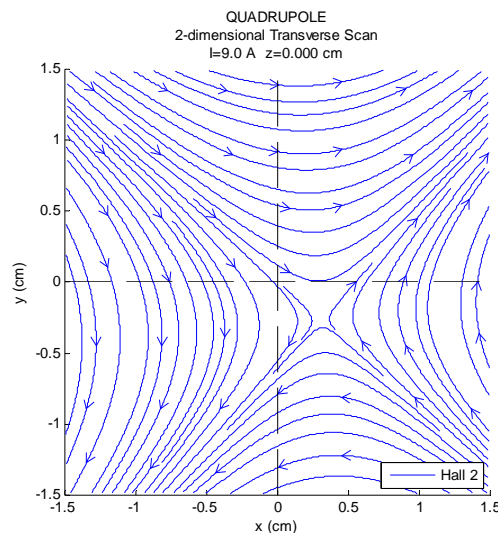


Figure 23: 2D Transverse Scan at $z=0$ (Hall 2)

Hall 2 was at a slight angle compared to Hall 1, which was why only data from Hall 1 was used to calculate the skew angle. This small angle is evident in this figure as the field seems to be rotated slightly. In addition, there is an origin mismatch of equal magnitude but opposite direction from Hall 1, as expected.

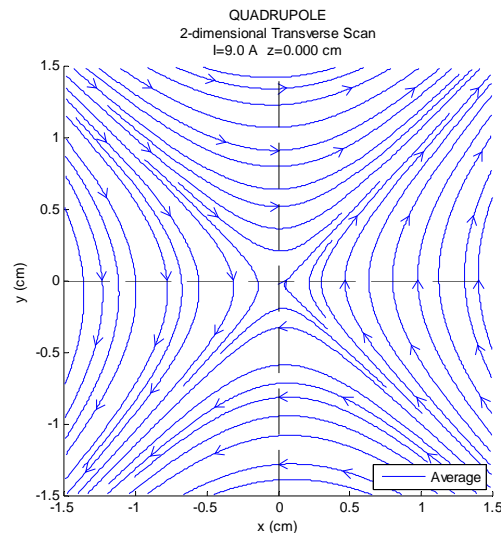


Figure 24: 2D Transverse Scan at z=0 (Average)

Although this figure is not an accurate depiction of the field with respect to the yoke since it includes the skewed data from Hall 2, it does demonstrate that the origin mismatch is due almost exclusively to the distances between the center of the probe arm and the active areas of the probes. This is seen by the fact that when the two probe values are averaged, the origin falls where it would if the arm was centered with the magnet.

Particle Trajectory Simulation

As a follow up to the mapping of the dipole magnets, a simple script was written to predict the trajectories taken by electrons through the mapped field. Time-stepping and space-stepping techniques were explored. All simulations were run through MatLAB, which was used to calculate and create a three dimensional plot of the particle trajectory.

A first attempt to accurately predict particle trajectories was accomplished using time-stepping numerical methods. It was assumed that the magnetic field was uniform over all space, and the electron was given a well defined initial position and momentum. The Lorentz force equation was then implemented to estimate the change in momentum induced by the magnetic field. Motion was tracked as a function of time, small steps in position associated with small time increments. The implicit Euler method was used, with velocity averaged between the initial and first-estimate positions. This code also implemented local error constraints defined by the magnitude of the momentum vector. Since the magnetic field can do no work, the magnitude of the particle's momentum must be conserved in time. The error measurement read the percent change in this quantity and was used to optimize the step size. The technique correctly predicted trajectories through constant magnetic fields.

However, the time stepping calculations assumed classical mechanics, which would not be valid for beam particles. Also, the time taken to execute the calculations grew rapidly as the number of steps increased. Therefore, this method was determined to be rather inefficient and an alternative method was pursued.

A space-stepping procedure was then utilized in order to increase efficiency in the code. This script assumed that the size of the position change was small enough that the magnetic field was constant throughout the region. Then, using the analytic solution to motion in a constant magnetic field, the new position and momentum were determined. In this approximation, the position and momentum changes can be calculated for an arbitrary magnetic field direction. This led to greater accuracy and efficiency in calculations. The computations were consistent with relativistic electrodynamics and predicted the particle's trajectory with extreme accuracy.

The final evolution of the code was to create a way of determining an average local field from a set of discrete measurements distributed over a three dimensional lattice. The method used involved locating the cell in which the particle resided. An interpolation was then conducted to find the local magnetic field at the particle's position. This interpolated value was then returned to the script and assumed to be constant over the small region. The magnetic field was only measured in one direction (B_y), and so the field was taken to have the form $\vec{B} = (0, B_y(x, y, z), 0)$. The field values were stored in an m-n-p array, with reference vectors correlating the physical position to the index of the array. If the particle left the region in which the field was mapped, a warning was returned to the user and the field value was set to zero.

To compute the effective length of the dipole, the change in position between steps was recorded along with the interpolated local value of the magnetic field. The two vectors were then multiplied and summed, resulting in a rectangular approximation to the integral. The approximation should be rather accurate since the simulation ranged over roughly 60 cm (the extent of the field map). The script was run with a step size of 2.5 mm and smaller, but it was found that the effective length converged to $L_e = 31.54 \text{ cm}$ with a step size of 2.5 mm.

This procedure was used to find the effective length for a bend angle of 20° , as reported. Since the magnitude of the magnetic field was fixed at the measured values, the momentum was varied until the proper bend angle was found. Trial and error lead to a bend angle of 20.02° with an initial momentum of $p_0 = (0, 0, 47.8995 \text{ MeV}/c)$.

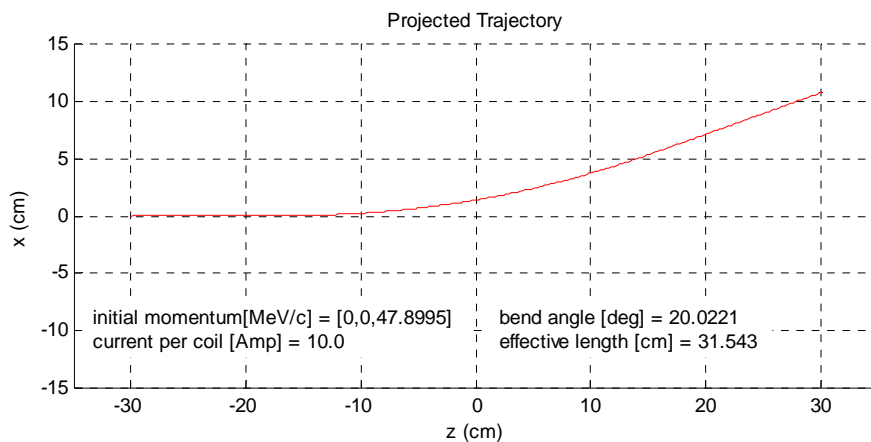


Figure 25: Momentum Varied Simulated Trajectory

Another method of producing the desired bend angle is to adjust the current per coil supplied to the dipole while holding the particle momentum fixed. This was also implemented, with the assumptions that the field did not saturate over the range of current used and that the magnet was properly de-gaussed beforehand. If the magnet did not saturate, then the magnetic field should grow linearly with current.

$$B_y = \left(\frac{\partial B}{\partial I}\right) I + B_0$$

Where B_0 represents the residual field in the magnet. If the dipole was properly de-gaussed, then it can be assumed that $B_0 = 0$. Therefore, with the above assumptions, and knowledge of the field value at given current allows for computation of the field value at any other current.

$$B = \left(\frac{I}{I_0}\right) B_0$$

Since the field map was known to be conducted at 10.0 A, this relation allowed for a normalization factor to be computed to find the field value for other currents.

The script required the user to define the initial position, initial momentum and a desired bend angle. It then repeatedly solved for the trajectory of the particle through the dipole field while varying the current. Thus, the script was able to specify the current per coil in the dipole needed to produce a given bend angle holding the initial momentum constant. The final bend angle was required to match the desired angle to an accuracy of $\pm 0.05^\circ$. This method was also used to compute the effective length of the magnet, with identical results as before. It was found that for an electron with $p_0 = (0, 0, 8 \text{ MeV}/c)$, the current per coil for a 20.0187° bend was 1.67 A . This script may be more useful, as long as the assumptions used are not violated.

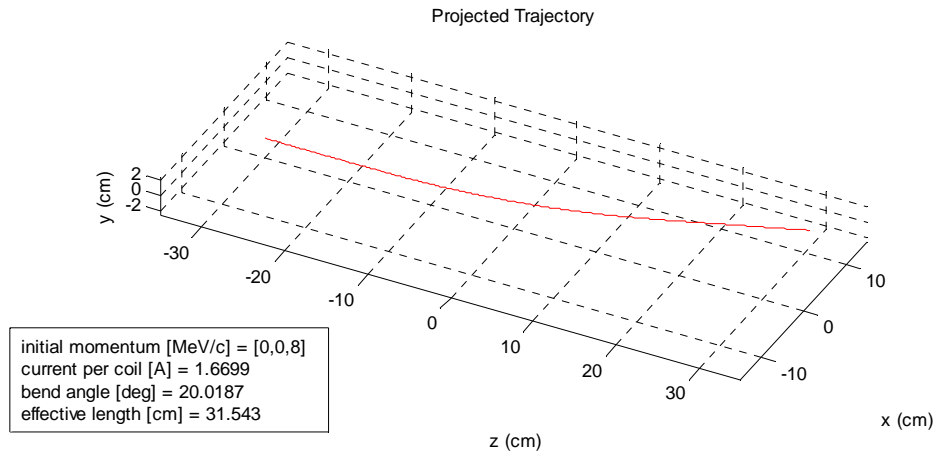


Figure 26: Current Varied Projected Trajectory

Both space-stepping procedures were capable of solving for beam trajectory with arbitrary initial momentum. Transverse momentum could be introduced with no loss of accuracy, and if the particle hit the beam pipe, then a warning was returned to the user. As shown, three dimensional plots were created for the predicted trajectories.

Conclusions

Extensive measurements were made of two Radiabeam magnets. Vendor simulation was confirmed and pertinent properties of these magnets were calculated. The effective lengths for the dipole and quadrupole were found to be 31.54 cm and 10.97 cm, respectively. Likewise, the quality of these magnets was demonstrated in that their fields were tightly constrained to be within the physical extent of the magnets. Furthermore, procedures for aligning these magnets accurately and measuring their properties to high precision were developed and implemented. These procedures were validated by the quality of data produced. Lastly, a script was constructed to produce accurate trajectory predictions and could be used to solve for a particle’s path through an arbitrary field.

Appendix A: Compumotor 4000 Motion Control Operation Guide

Initialization from De-energized State

This outlines a procedure for initializing the Compumotor device so that it can be controlled remotely through the GPIB cable.

To ready the device from de-energized state¹:

Turn on device. The power switch is behind the z-axis motor.

Select ACCESS

Input 4000

Press ENTER

Press MAIN MENU

Select IMMED

Select DEFINE

Select GPIB

Select SRQ

Select N for all

Press ENTER

Select DEFINE

Select GPIB

Select ADDR

Enter 8

Press ENTER

Select DEFINE

Select GPIB

Select ERR_MSG

Select OFF

Press ENTER

Select DEFINE

Select GPIB

Select PROMPTS

Select OFF

Press ENTER

The device is now formatted to use the GPIB cable

Manual Positioning

To program the device so that it can be positioned from the IMMED menu, the following program must be stored on the device. If the Compumotor 4000 is to be used with the automated stepping program (2DquadScan.vi), then the following program will be loaded automatically when program is executed. The position will be displayed in centimeters². From the Main Menu:

Select EDITOR

Select ALPHA

¹ From a de-energized state, turning the machine on is all that is needed to use the jog mode: press JOG MODE from the main menu, and then use arrows

² If the program is entered manually, position resolution will be decreased as only one decimal place will be available when entering the "UNIT POS" command

Input MOVE3D using ARROW KEYS and NUMBER PAD
Press ENTER
Select INSERT
Press ENTER

Input the following commands as shown

```

MODE E_ABS E_ABS E_ABS *
ENCO ERES 2000 1016 1016 *
UNIT POS 3937.0000 2000.0000 2000.0000 *
VEL 200000 200000 200000 *
ACCEL 50000 50000 50000 *
DECEL 50000 50000 50000 *
DISPLAY ON LCD3 EABS EABS EABS *
MOVE Q11 Q12 Q13 *
*

```

Press MENU RECAL to return to MAIN MENU

The device can now be positioned using the IMMED/MOVE menu.

Sample Manual Stepping Programs

The following two programs step the probe by declared step sizes. Both programs require MOVE3D to function. STEPZ steps through z at a fixed (x, y). STEPSTER steps through (x, y, z) within a set area of (x, z) space, but no limit is placed on y-space. Both are designed to facilitate repeated stepping by a fixed amount. These programs are already loaded onto the controller, but can be easily changed to suit a given measurement.

These programs ease the process of moving the device repeatedly by a fixed amount, but do not record data. When these programs are used, all data must be recorded by hand.

STEPZ

```

MODE E_INC E_INC E_INC *
LABEL LABEL1
WAIT FOR F-KEY6 TO BE PRESSED
MOVE Q1 * * *
GOTO LABEL1

```

This program requires the definition of [Q1 = step size]

STEPSTER

```

MODE E_ABS E_ABS E_ABS *
MOVE 0 0 0 *
MODE E_INC E_INC E_INC *

LABEL STEPZZ
OUT LCD2, 01 ^PRESS F6^
WAIT FOR F-KEY6 TO BE PRESSED
MOVE Q1 * * *
ON E_ABS1 > Q2 GOTO STEPXX
GOTO STEPZZ

```

```

LABEL STEPXX
MODE      E_ABS *           *           *
MOVE      0                Q1          *           *
MODE      E_INC            *           *           *
ON        E_ABS2> Q3       GOTO        STEPYY
GOTO      STEPZZ

LABEL STEPYY
MODE      E_ABS E_ABS *           *
MOVE      0                0          Q1          *
MODE      E_INC            E_INC      *           *
GOTO      STEPZZ

```

This program requires the definition of:

- [Q1 = step size]
- [Q2 = z-limit + Q6]
- [Q3 = x-limit + Q6]
- [Q4 = y-limit + Q6]
- [Q6 = Q1 / 2]

Automated Program 2DquadScan.vi

This program (2DquadScan.vi) runs through LabVIEW. The red boxes in the window are the inputs that should be varied:

(z initial, z final, dz, y pos, x initial, x final, dx).

The signs of *dz* and *dx* must match the directions in which the probes are to move. For example, if *(z initial = 0)*, *(z final = -5)*, and the step size is *0.5*, then *(dz = -0.5)*.

These parameters should be set appropriately for the magnet, with numerical values reported in centimeters. Be sure to account for the width of the probe arm when setting parameters so that the device does not collide with the magnet. This program reports the command positions, as oppose to measured positions. It should then be expected that the reported positions are in error within the tolerance of the encoder (~20 μm).

The program scans in a (x, z) plane within the stated boundaries, and records the reading on each hall probe at every location. This data is then saved in a .txt file.³ The file can be saved in any desired location by changing the file path in the program window.⁴ This file can then be opened in excel and formatted as desired. When prompted, the .txt file is "tab delimited," and choosing this option will automatically sort data into correct columns.

To run a scan, open 2DquadScan, which is saved on the RF lab computer under Desktop\Hall Probe\2DquadScan.vi. Change the parameters of the scan and make sure the remote controller of the positioning device is at the MAIN MENU. If the device is not at the Main menu, there can be an error in running the program. If an error does occur, stop the program in LabVIEW and press MENU RECALL until at the Main menu. Start the program in LabVIEW, and wait for data to be collected. The program may not run even when the controller is at the Main menu screen. In this case, stop the program and press MENU RECALL several times. Then restart the program. Repeat until the program runs.

If any problems arise with the program, the author is Chuck Doose of the Advanced Photon Source (APS) facility.

³ Column headings are not saved to .txt file and will have to be added. The column order is z, x, y, Hall 1, Hall 2.

⁴ As currently set, the file will be saved as: C:\Documents and Settings\adminawa\Desktop\Hall Probe\Data\Scan1.txt.

Useful Commands and Functions⁵

JOG MODE

Jog mode can only be accessed from the Main menu. If the controller is on a different menu, press MENU RETURN until the Main menu is displayed. Then press JOG MODE to enter Jog mode. In Jog menu, the device can be moved using the arrow keys. The LCD displays which axis is currently assigned to which arrow keys. To change these assignments, press the function key below either L/R or U/D and enter the number of the axis desired (z=1, x=2, y=3). Select the desired speed by pressing the function button below either High or Low. These speeds can be changed under the DEFINE menu⁶. To exit Jog mode, press MENU MODE.

MENU MODE

Menu mode allows the user to access all the functions built into the Compumotor 4000, and any user defined programs. The only program that is automatically loaded onto the device (from a de-energized state) is POWER_UP, which is stored as ROM. From the Main menu, use the function keys to navigate through the menus to find the desired function. If there are more options than can be displayed over the function keys at one time, either use the ...ETC key to advance to the next set, or use the U/D arrows to navigate.

EDITOR

This menu allows the user to edit programs stored in the RAM of the controller.

To write a new program, select EDITOR, then press ALPHA and use the arrow keys/number pad to enter the name of the new program (program names must start with a letter). After the name has been entered, press ENTER, and then INPUT to begin writing. Select the command using the function keys. To save a new program, press MENU RECALL.

To edit an existing program, scroll through the list of programs until the desired program is found, then press ENTER. Scroll through the program and use the INSERT, EDIT, FIND, DELETE and COPY commands to edit the program. To save an edited program, press MENU RECALL. The new program can be saved in addition to the old program, it can replace the old program or the edited version can be discarded. Select the desired save option and press enter.⁷

RUN

The run menu allows for execution of programs stored on the controller. Select RUN from the Main menu and then scroll through the program list. Once the desired program is found, press enter. The controller then prompts the user to define the scope of the program to be executed. For example, to execute the entire program, select

RUN FROM BEG UNTIL END

IMMED

This menu allows for immediate execution of a command line. All functions available under the IMMED menu can be written into programs using the EDITOR menu. After selecting IMMED, scroll through the listed functions until the desired action is found. Below are some commonly used functions under the IMMED menu.⁸

⁵ If a menu/function/command is not listed here, reference Compumotor 4000 User Guide, Chapter 3.

⁶ Reference Compumotor 4000 User Guide, Chapter 3 for a full description of DEFINE.

⁷ For advice on writing programs, reference Compumotor 4000 User Guide, Chapters 3 and 4.

⁸ For a description of all functions under IMMED, reference Compumotor 4000 User Guide, Chapter 3.

DISPLAY

The Display menu allows the LCD display to be changed. The LCD is divided into rows (1 through 4), each with 40 characters. To set an LCD display, enter the row number and the values to be displayed. Like other menus, the axes progress from left to right. For example, to display the Encoder ABSolute position for axis 1, the Encoder INCRemental position for axis 2 and the Motor ABSolute position for axis 3 on the third LCD row, the following command should be entered

```
DISPLAY ON LCD3      EABS      EINC      MABS      *
```

Be sure to tab to the appropriate point (denoted by *) before entering the desired values. If the values are not entered in appropriate locations an error code will appear.

If the displayed position does not change when the device is moving, then the display will need to be reset. This can be done from the IMMED menu with the command shown above.

MODE

This menu controls the interpretation of the values input under the MOVE menu. Mode can be set to Motor ABSolute, Motor INCRemental, Encoder ABSolute and Encoder INCRemental. The most common mode setting will be E_ABS, and with the parameters defined as they are in MOVE3D, the numerical values will be in centimeters. E_INC can also be useful for stepping the device through an axis.

MOVE

This menu allows for positioning the device. Input will be interpreted differently depending on the MODE setting. For E_ABS, the device will be moved to the input position with respect to the defined zero point. For E_INC, the device will be deflected by the input amount from its current position. M_ABS and M_INC are analogous, but deal with the number of motor steps rather than the position as read by the encoder. Again, the axes run from 1 to 4 starting at the left. Be sure to input the desired values in the correct locations.

PDEF

This menu allows for the definition of the devices current position. The definition can be any value desired. Enter the value to be assigned to that position in the correct positions and press enter to assign those values. This command is useful in that once the center of a magnet is found, that position can be defined as zero and the device moved relative to that point.

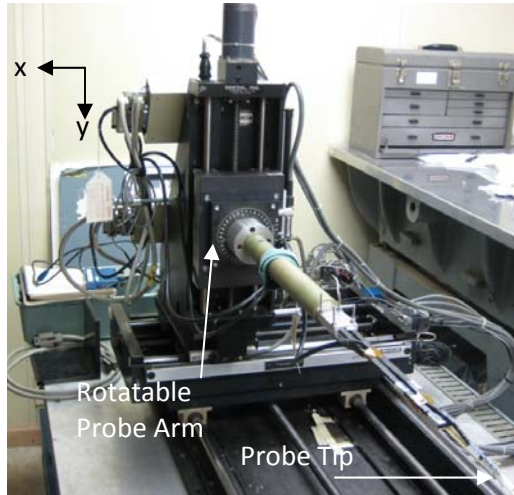
MATH

Math allows for definition of variables to be used. To assign a value to a variable, press MATH and enter the number of the variable and the value to be assigned to it. Q1-Q99 are reserved for numerical values, while Q100 and above are reserved for character strings. For example, to assign the value (5 + 2) to Q1, the following should be entered

```
MATH Q1 = 5      +      1
```

Definitions of variables can also include other variables, as long as the referenced variable is defined. For example, the definition (Q1 = 5 + Q2) is entered with:

```
MATH Q1 = 5      +      Q2
```

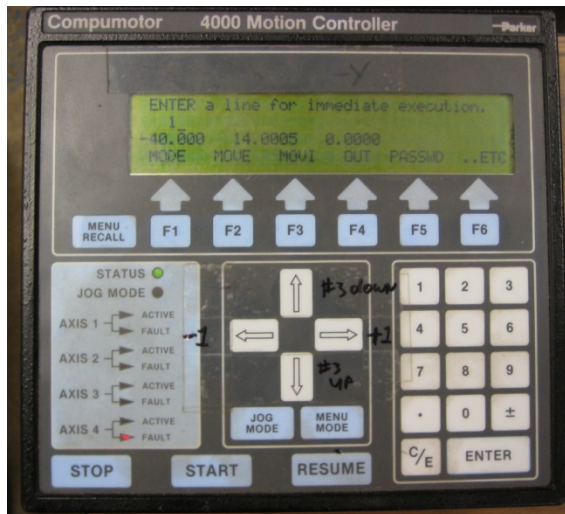
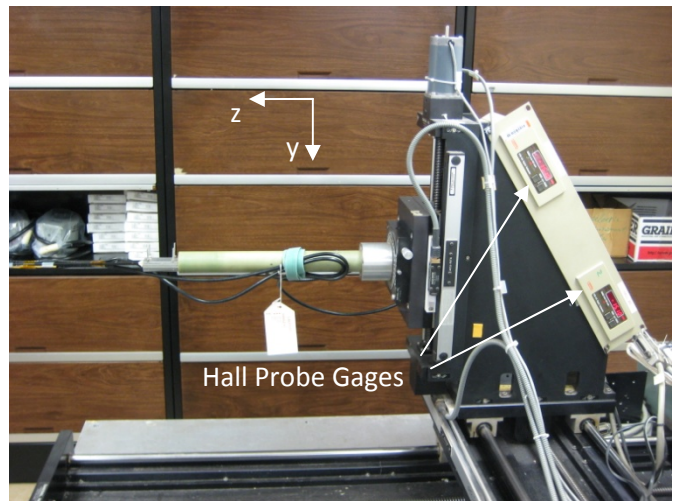


Front view of the device

Notice the tick markings at the base of the probe arm. These mark the amount of rotation of the arm. Also, note the large number of wires behind the device. Make sure these to not become entangled as the device moves.

Side view of the device

The hall probe gages are visible here on the right side of the device. Axis one has a very large range, but be careful not to extend the probe arm too far into the magnet, as parts of the device may collide with the magnet.



Control Panel

Note the function keys immediately below the LCD display, and the arrow pad. The fault indicator for axis four is lit because there is no axis connected to that port. The current menu displayed is IMMED, from which the device can be moved to a specified location.

Appendix B: Physics of Space-Step Simulation

The script assumes that the magnetic field varies slowly enough so that it can be considered constant over the step size taken. This small step size (L) is chosen to make this assumption true. L is the displacement between two consecutive positions, not the path-length of the trajectory. In addition, it is useful to consider a rotated coordinate frame. The origin of this rotated frame is the point where the particle resides at the beginning of the iteration.

For any magnetic field vector, there will be two components of the momentum vector, one parallel to the field and one perpendicular to it. The magnetic force will only act to change that part of the momentum that is perpendicular to the magnetic field.

Define the transverse momentum as (p_t) and the parallel momentum as ($p_{||}$) such that ($p = p_t + p_{||}$). These can be computed as follows

$$p_{||} = (p \cdot B) \frac{\vec{B}}{B} \quad | \quad \vec{B} = \frac{B}{B}$$

and

$$p_t = p - p_{||}$$

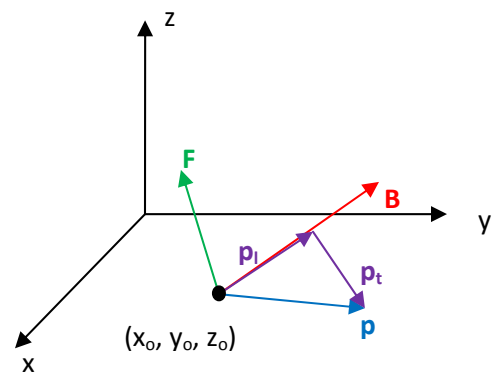
To create the rotated frame, the axes are defined so that

$$xx \parallel p_t$$

$$yy \parallel B$$

$$zz \parallel p \times B$$

which is the direction of the force on a positive charge. All equations are written implicitly for a positive charged particle, but negative particles are accommodated by the definition of $d\theta$ and ρ .



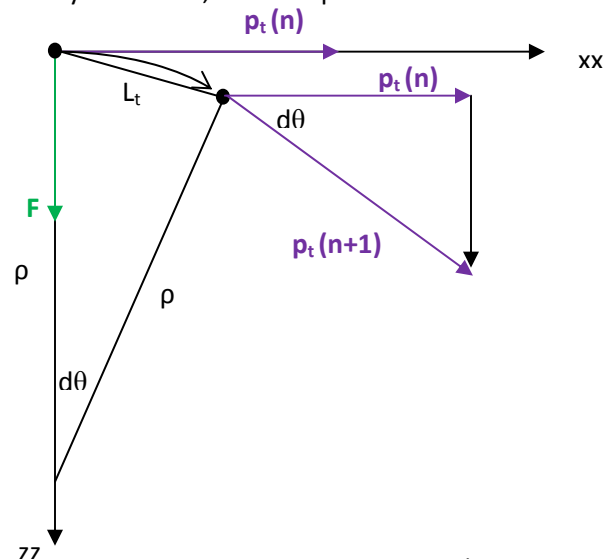
The solution for motion of a charged particle in a uniform magnetic field is a helix. This collapses to a circle in the transverse plane (xx, zz). Using the known geometry of a circle, the new position and momentum can be found in the curvilinear frame (xx, yy, zz).

$$\rho = \left| \frac{p_t}{qB} \right| \quad \text{is the radius of curvature}$$

$$L_t = \left(\frac{qBL}{p} \right) L \quad \text{is the displacement in the transverse plane}$$

$$L_t^2 = 2\rho^2 - 2\rho^2 \cos(d\theta)$$

$$\begin{aligned} \cos(d\theta) &= 1 - \frac{L_t^2}{2\rho^2} \\ &= 1 - \frac{1}{2} \left(\frac{qBL}{p} \right)^2 \\ &\approx 1 - \frac{1}{2} \theta^2 \end{aligned}$$



for small values of $d\theta$. If the step size is chosen appropriately, then this assumption is valid. Therefore

$$d\theta = \pm \frac{qBL}{p}$$

The ambiguity in the sign of $d\theta$ is due to the sign of the charge. As drawn, the force direction is appropriate for a positive charge. If the charge is negative, then the particle will bend in the other direction. Simple observation shows that the equations remain identical except that $d\theta \rightarrow -d\theta$ and $p \rightarrow -p$. Therefore, by leaving the angle as

$$d\theta = \frac{qBL}{p}$$

and the radius of curvature as

$$\rho = \frac{p_t}{qB}$$

the sign of the charge yields the correct signs for $d\theta$ and ρ . Again, these values are for the frame constructed as shown, with $(zz \parallel p \times B)$ and therefore zz is anti-parallel to the force on a negative charge. Using the above definitions the position in the rotated frame can be defined for either a positive or negative charge as

$$xx = \rho \sin(d\theta)$$

$$zz = \rho [1 - \cos(d\theta)]$$

$$yy = \left(\frac{p_t}{p}\right)L$$

Likewise, the new momentum vector is

$$p_{xx} = p_t \cos(d\theta)$$

$$p_{zz} = p_t \sin(d\theta)$$

$$p_{yy} = p_t$$

Now, the new position and momentum have been defined in terms of the initial position, initial momentum and field strength. All that remains is to transform the (xx, yy, zz) coordinates into the (x, y, z) frame. Knowing that $(xx \parallel p_t)$, $(yy \parallel B)$ and $(zz \parallel p \times B)$, the rotation matrix is constructed as shown.

$$\lambda = \begin{bmatrix} \frac{(p_t)_x}{p_t} & \frac{B_x}{B} & \frac{p_y B_x - p_x B_y}{p_t B} \\ \frac{(p_t)_y}{p_t} & \frac{B_y}{B} & \frac{p_x B_x - p_y B_y}{p_t B} \\ \frac{(p_t)_z}{p_t} & \frac{B_z}{B} & \frac{p_x B_y - p_y B_x}{p_t B} \end{bmatrix}$$

such that

$$\begin{bmatrix} x \\ y \\ z \end{bmatrix} = \begin{bmatrix} x_0 \\ y_0 \\ z_0 \end{bmatrix} + \lambda \begin{bmatrix} xx \\ yy \\ zz \end{bmatrix} \quad \text{and} \quad \begin{bmatrix} p_x \\ p_y \\ p_z \end{bmatrix} = \lambda \begin{bmatrix} p_{xx} \\ p_{yy} \\ p_{zz} \end{bmatrix}$$

Implementing this procedure during each iteration allows for a numerical solution of the trajectory through an arbitrary field. However, the field must be defined at each point for this procedure to work. This was accomplished by interpolating between eight values, each corresponding to one corner of a unit cell of a three dimensional lattice. Field measurements were made at the corners of a lattice, and using the position of the particle, a local magnetic field was interpolated from the closest corners in the lattice. This interpolation is achieved by `getBycurrent.m`, as shown below.

Appendix C: Construction of Data File for Simulation

The output of `2DquadScan.vi` is a `.txt` file with five columns, as discussed above. This `.txt` file will be a planar scan at a fixed elevation. The data must be put into an `n-p` array, with reference vectors `xref` and `zref` such that `length(xref)=p` and `length(zref)=n`. once this has been done for all horizontal planes to be included in the final map, `Bgrid` can be constructed. A reference vector `yref` must be created, storing the elevations of the planes mapped in order from lowest (most negative) to highest (most positive). Then, `Bgrid` is constructed by repeatedly assigning the appropriate `n-p` array to the index corresponding to its elevation. This then produces the final `m-n-p` array with `length(yref)=m`, `length(zref)=n` and `length(xref)=p`. The array and all three reference vectors need to be saved to some `.mat` file. In order to use this data, be sure to edit `getBycurrent.m` so that it loads the correct data.

Appendix D: MatLAB Script Used in Current Varied Simulation

These MatLAB scripts and functions were used simulate the path of a beam particle through a dipole field. The measured field strengths were modulated by a normalized current. This allowed the script to solve for the current per coil to achieve a certain bend angle with a specified initial momentum. For these scripts to function, the data must be stored as a `.mat` file with the format described in `getBycurrent.m`.

givemecurrent.m

```
%this script written to find the current needed in a dipole to produce a
%given bend angle with a known initial position and momentum
%written by Reed Essick for AWA group
```

```
%this script assumed the length (L) is short enough that the magnetic field
%is constant over it, and then determines the new position and momentum of
%the particle. equations assume relativistic mechanics and the lorentz
```

```

%force law hold.

%characteristics of the particle and field are defined within this script.
%the initial conditions of the motion are also defined within the script.

clear all; close all;
x=input('initial position [cm] = ');
po=input('initial momentum [MeV/c]= ');
thetad=input('desired bend angle [degrees] ');

%assuming that there is no saturation (correct up to at least 10 A), then
%the field varies linearly with current as: B=m*I+Bo.
%if the magnet has been de-gaussed properly, then Bo=0. this then yields
%the following relation: B=m*I
%from this, it can be shown that the field value at any current can be
%found using the field value at a known current. Bgrid was taken at I=10 A,
%so for any current besides I=10 A, the field should look like
%B=(I [A]/10)*Bgrid

%define initial guess for current I
I=5; %Amps

%compute theta using initial guess for current
[theta,Leff,xt,yt,zt]=current_func(x,po,I);

while abs(theta-thetad)>0.05,
    if theta>thetad
        I=(4/5)*I;
        [theta,Leff,xt,yt,zt]=current_func(x,po,I);
    else
        I=(6/5)*I;
        [theta,Leff,xt,yt,zt]=current_func(x,po,I);
    end
end

disp('current supplied to magnet [A]= ')
disp(I)
disp('bend angle [degrees]= ')
disp(theta)
disp('effective length of dipole [cm]= ')
disp(Leff)

%plot trajectory
plot3(zt*100,xt*100,yt*100,'-b','markersize',5,'linewidth',1);
xlabel('z (cm)');ylabel('x (cm)');zlabel('y (cm)');title('Projected
Trajectory');
grid on;
axis equal;
view(2);

current_func.m

function [theta,Leff,xt,yt,zt]=current_func(x,po,I)

%this function written to return the bend angle of a particle passing

```

```

%through a dipole field.
%written by Reed Essick for AWA group

%x must be in centimeters
%po must be in MeV/c
%I must be in Amperes

%this script assumed the length (L) is short enough that the magnetic field
%is constant over it, and then determines the new position and momentum of
%the particle. equations assume relativistic mechanics and the lorentz
%force law hold.

%characteristics of the particle and field are defined within this script.

%assuming that there is no saturation (correct up to at least 10 A), then
%the field varies linearly with current as:  $B=m*I+Bo$ .
%if the magnet has been de-gaussed properly, then  $Bo=0$ . this then yields
%the following relation:  $B=m*I$ 
%from this, it can be shown that the field value at any current can be
%found using the field value at a known current. Bgrid was taken at  $I=10$  A,
%so for any current besides  $I=10$  A, the field should look like
%B=(I [A]/10)*Bgrid

%after this point, SI units are used throughout this script

%define initial position and momenta
S.r=x/100; %[meters]
S.p=po*5.344285412276782*10^-22; %[kg(m/s)]
S.P=norm(S.p);

%define charge of particle
q=-1.60217646*10^-19; %[Coulombs]

%define step length
L=2.5*10^-3; %[meters]

for n=1:247
    %get Bvector from position
    By=getBycurrent(S.r(n,1)*100,S.r(n,2)*100,S.r(n,3)*100); %Gauss
    Blocal(n)=(I/10)*By; %Gauss
    B=[0,Blocal(n),0]/10000; %Tesla

    if norm(B)==0
        %if norm(B)==0, then the particle is not deflected
        S.r(n+1,:)=S.r(n,:)+L*(S.p(n,:)/norm(S.p(n,:)));
        S.p(n+1,:)=S.p(n,:);
        S.P(n+1)=S.P(n);

    else
        %determine the longitudinal and transverse components of momentum
        pL=dot(S.p(n,:),B)*(B/(norm(B))^2); PL=norm(pL);
        pT=S.p(n,:)-pL; PT=norm(pT);

```

```

YY
    %the co-moving frame is constructed so that xx lies parallel to pT,
    %lies parallel to B and zz lies parallel to F=q*cross(pT,B)

    if PT==0
        %if PT==0, then the particle is not deflected
        S.r(n+1,:)=S.r(n,:)+L*(S.p(n,:)/norm(S.p(n,:)));
        S.p(n+1,:)=S.p(n,:);
        S.P(n+1)=S.P(n);

    else
        %determine the new coordinates in the co-moving rr frame
        SS.rr(1,1)=(PT/(q*norm(B)))*sin((q*norm(B)*L)/S.P(n));
        SS.rr(1,2)=(PL/S.P(n))*L;
        SS.rr(1,3)=(PT/(q*norm(B)))*(1-cos((q*norm(B)*L)/S.P(n)));

        %define the new momenta in the co-moving rr frame
        SS.pp(1,1)=PT*cos((q*norm(B)*L)/S.P(n));
        SS.pp(1,2)=PL;
        SS.pp(1,3)=PT*sin((q*norm(B)*L)/S.P(n));

        %define rotation matrix for coordinate transformation
        lambda=[ pT(1)/PT , B(1)/norm(B) , (S.p(n,2)*B(3)-
S.p(n,3)*B(2))/(PT*norm(B)) ;
                pT(2)/PT , B(2)/norm(B) , (S.p(n,3)*B(1)-
S.p(n,1)*B(3))/(PT*norm(B)) ;
                pT(3)/PT , B(3)/norm(B) , (S.p(n,1)*B(2)-
S.p(n,2)*B(1))/(PT*norm(B)) ];

        %convert rr coordinates into r coordinates
        ab=lambda*transpose(SS.rr);
        S.r(n+1,:)=S.r(n,:)+transpose(ab); %the rr frame coordinates
represent the change in position, and therefore are added to the previous
position in the r frame

        %convert rr momenta into r momenta
        b=lambda*transpose(SS.pp);
        S.p(n+1,:)=transpose(b); %the rr momenta correspond to the total
momenta of the particle and therefore replace the previous set of r momenta
        S.P(n+1)=norm(S.p(n+1,:));

    end

end

end
dsvec(n,:)=(S.r(n+1,:)-S.r(n,:)); %meters
ds(n)=sqrt(sum(dsvec(n,:).^2)); %meters

%define a measure of error
%error(n+1,1)=(S.P(n+1)-S.P(1))/S.P(1); this error is meaningless since
%the magnitude of momentum is kept constant. all this would measure is
%rounding error

end
%compute bend angle
pf=S.p(end,:)/(5.344285412276782*10^-22); %MeV

```

```
theta=acos(sum(po.*pf)/(sqrt(sum(po.^2))*sqrt(sum(pf.^2))))*180/pi; %degrees
```

```
%implement procedure to adjust current to find desired theta
```

```
%compute the effective length
BL=sum(ds.*Blocal); %Gauss
Bmax=max(Blocal); %Gauss
Leff=BL*100/Bmax; %centimeters
```

```
xt=S.r(:,1);yt=S.r(:,2);zt=S.r(:,3);
```

getBycurrent.m

```
function By=getBycurrent(x,y,z)
%this function written to interpolate the value of By from discrete values
%at known positions. god save the queen
%written by reed essick for awa group
```

```
%load the data file that stores the By values in a m-n-p array named Bgrid
with
%reference vectors x-y-z
%length(x)=p; length(y)=m; length(z)=n;
load Bgrid.mat;
```

```
%find the index of the closest corner in the 3D-lattice of By values. this
%corner will be (ny,nz,nx)
nx=find(abs(x-xref)==min(abs(x-xref)));nx=nx(1);
ny=find(abs(y-yref)==min(abs(y-yref)));ny=ny(1);
nz=find(abs(z-zref)==min(abs(z-zref)));nz=nz(1);
```

```
%find the next nearest corner in the 3D-lattice of By values. this corner
%will be (nyy,nzz,nxx)
```

```
if x-xref(nx)>=0
    nxx=nx+1;
else
    nxx=nx-1;
end
if y-yref(ny)>=0
    nyy=ny+1;
else
    nyy=ny-1;
end
if z-zref(nz)>=0
    nzz=nz+1;
else
    nzz=nz-1;
end
```

```
%check to make sure that the point is still within the bounds of the array
if nxx>length(xref)|nxx<=0
    By=0;
    %disp('PARTICLE HIT PIPE WALL');
else
    if nyy>length(yref)|nyy<=0
        By=0;
```

```

        %disp('PARTICLE HIT PIPE WALL');
    else
        if nzz>length(zref)|nzz<=0
            By=0;
            %disp('PARTICLE HAS LEFT THE DIPOLE FIELD');
        else
            %interpolate over y. this is done first because it is expected
that there
            %is very little variation over y.
            %a better way to do this would be to find the differences between
the
            %closest and second closest points and interpolate first over the
direction
            %with the smallest variation, then the second smallest and
finally over the
            %direction with most variation
            Bnxnz=(Bgrid(ny,nz,nx)-Bgrid(nyy,nz,nx))/(yref(ny)-yref(nyy))*(y-
yref(nyy))+Bgrid(nyy,nz,nx);
            Bnxxnz=(Bgrid(ny,nz,nxx)-Bgrid(nyy,nz,nxx))/(yref(ny)-
yref(nyy))*(y-yref(nyy))+Bgrid(nyy,nz,nxx);
            Bnxnzz=(Bgrid(ny,nzz,nx)-Bgrid(nyy,nzz,nx))/(yref(ny)-
yref(nyy))*(y-yref(nyy))+Bgrid(nyy,nzz,nx);
            Bnxxnzz=(Bgrid(ny,nzz,nxx)-Bgrid(nyy,nzz,nxx))/(yref(ny)-
yref(nyy))*(y-yref(nyy))+Bgrid(nyy,nzz,nxx);

            %now interpolate over x, which is expected to have the second
least
            %variation through the region of interest.
            Bnz=(Bnxnz-Bnxxnz)/(xref(nx)-xref(nxx))*(x-xref(nxx))+Bnxxnz;
            Bnzz=(Bnxnzz-Bnxxnzz)/(xref(nx)-xref(nxx))*(x-xref(nxx))+Bnxxnzz;

            %now interpolate over z, which is expected to hav eht most
variation
            By=(Bnz-Bnzz)/(zref(nz)-zref(nzz))*(z-zref(nzz))+Bnzz;
        end
    end
end
%and there you have it

```